Temperature Dependence of O(^{1}D) Quantum Yields from the Photolysis of Ozone between 295 and 338 nm

Geoffrey D. Smith, Luisa T. Molina, and Mario J. Molina*

Departments of Earth, Atmospheric and Planetary Sciences and of Chemistry, Massachusetts Institute of Technology, Cambridge, Massachusetts 02139

Received: March 16, 2000; In Final Form: July 25, 2000

The O(^{1}D) quantum yields from the photolysis of ozone (O_3) have been measured in the wavelength range 295−338 nm at temperatures of 226−298 K using chemical ionization mass spectrometry (CIMS). In the 312−324 nm range, the quantum yield was found to be temperature dependent, implying that internal energy in O_3 accounts for some of the O(^{1}D) production at wavelengths beyond the thermodynamic threshold of 310 nm. In the 328−338 nm range, the quantum yield is nearly constant ($\Phi \sim 0.12$) and independent of temperature, suggesting that the "spin-forbidden" channel is active at these wavelengths and contributes to O(^{1}D) production beyond 310 nm. Using the quantum yields presented here results in a sizable increase in the calculated tropospheric O(^{1}D) production at large solar zenith angles.

Introduction

The absorption of light by ozone plays a very significant role in the chemistry of the atmosphere. In the stratosphere absorption of UV light by O_3 prevents short wavelength light from reaching the Earth's surface. Longer wavelength light ($\lambda > 300$ nm) that penetrates to the lower atmosphere can dissociate O_3 through the following four photolysis pathways:

$$O_3 + h\nu \rightarrow O(^1D) + O_2(^1\Delta_g) \qquad \lambda \leq 310 \text{ nm} \qquad (1)$$

$$\rightarrow O(^1D) + O_2(^3\Sigma_g^-) \qquad \lambda \leq 411 \text{ nm} \qquad (2)$$

$$\rightarrow O(^3P) + O_2(^1\Delta_g) \qquad \lambda \leq 612 \text{ nm} \qquad (3)$$

$$\rightarrow O(^3P) + O_2(^3\Sigma_g^-) \qquad \lambda \leq 1180 \text{ nm} \qquad (4)$$

The production of excited oxygen atoms, O(^{1}D), initiates oxidation and subsequent removal of pollutants through the formation of OH:

$$O(^1D) + H_2O \rightarrow OH + OH \qquad (5)$$

At wavelengths greater than 300 nm the solar actinic flux increases dramatically while both the O_3 absorption cross section and the O(^{1}D) quantum yield decrease substantially. Therefore, O(^{1}D) production in the atmosphere is influenced considerably by the value of the quantum yield in this region of the spectrum.[1]

The photolysis of ozone has been studied for decades, with much attention being paid to the measurement of O(^{1}D) yields.[2−13] Photolysis occurs predominantly through reaction 1 at $\lambda < 310$ nm, the thermodynamic threshold for this channel. However, O(^{1}D) quantum yields greater than zero have been measured at wavelengths as long as 336 nm,[9] although there is much discrepancy amongst various sets of measurements. Recent work has concentrated on quantitatively determining the yield in this "tail" region.[7,9−13] In addition, efforts have been made to identify the magnitudes of contributions from reaction 1 (spin-allowed) and reaction 2 (spin-forbidden) to O(^{1}D) yields in the tail region.[10−13] Takahashi et al.[13] recently used laser-induced fluorescence to detect both the O(^{3}P) and O(^{1}D) photofragments directly at 305−329 nm at several temperatures, and they were able to assign O(^{1}D) yields from both reactions 1 and 2. Using resonance fluorescence to detect O(^{1}D) quenched to O(^{3}P) and laser-induced fluorescence to detect O(^{1}D) as OH, Talukdar et al.[12] were also able to deduce O(^{1}D) yields at similar wavelengths and temperatures.

In an effort to further resolve the production of O (^{1}D) in this "tail" region of the spectrum, we have employed a broadband light source coupled to a monochromator for wavelength discrimination. Selective titration of O(^{1}D) with N_2O was used, and subsequent detection and measurement of the yields was accomplished with chemical ionization mass spectrometry (CIMS). Use of the monochromator reduced the light flux available for photolysis, but it offered continuous wavelength selection. The corresponding reduction in photolysis was compensated for by the high sensitivity of the CIMS detection technique.

Experiment

A schematic diagram of the Photo-CIMS experimental apparatus is shown in Figure 1. Ozone was produced by passing O_2 (UHP Matheson) through an ozonizer (OREC) and was then collected in a silica gel trap at 196 K. A 75 W xenon arc lamp (Oriel 6137) produced white light which was focused into a monochromator (McKee-Pedersen Instruments 1018B). The monochromator contained a diffraction grating (2360 lines/mm) which dispersed the light and allowed for wavelength selection. The photolysis tube (11 cm long) was positioned at the exit slit of the monochromator and was constructed from $^1/_4$ in. o.d. Pyrex tubing with quartz windows at each end. The light flux was measured at the end of the tube with a calibrated photodiode (Oriel 70282).

Ozone was introduced by passing a carrier flow of Ar (UHP Matheson) through the silica gel trap. The O_3/Ar flow (10 STP mL min^{-1}) and N_2O (UHP Matheson) flow (5 STP mL min^{-1}) entered and mixed at the rear of the photolysis tube. The concentration of O_3 in the photolysis tube, as measured through

10.1021/jp001006d CCC: $19.00 © 2000 American Chemical Society
Published on Web 09/13/2000

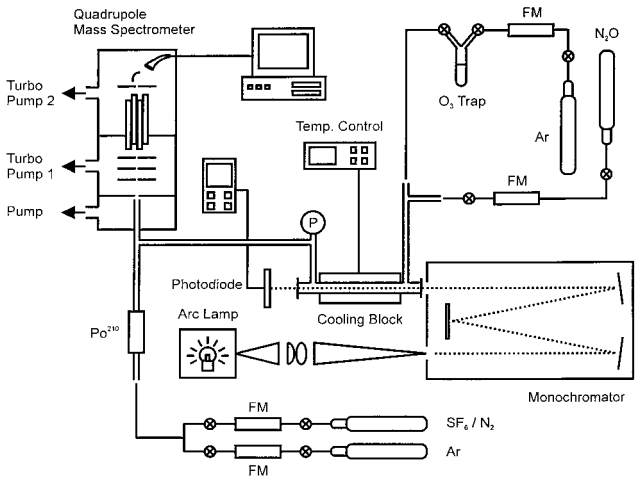

Figure 1. Schematic diagram of the apparatus used in this study.

UV absorption, was typically $(1-5) \times 10^{16}$ molecules/cm^3. The entire flow passed down the length of the tube, which was housed in an aluminum block used for temperature regulation. The block contained a reservoir for liquid nitrogen and four imbedded cartridge heaters which were connected to a temperature controller. The gas flow exiting the tube then entered the ion−molecule region which consisted of $^1/_4$ in. o.d. Pyrex tubing and a polonium ionization source (NRD Inc.) and was located orthogonally to the photolysis tube. A quadrupole mass spectrometer (ABB Extrel Merlin) was located at the end of the ion−molecule region. All gas flows were monitored with calibrated mass flow meters (Tylan). The pressures in the photolysis tube (∼50 Torr) and the ion−molecule region (∼25 Torr) were monitored using a 0−1000 Torr capacitance manometer (MKS Baratron).

The chemical ionization of the photolysis-titration product (NO_2) was achieved through a series of ionization reactions. As with some of our previous studies[14] the reagent ion SF_6^- was generated by passing a ∼5 STP L min^{-1} flow of Ar with SF_6 (∼1 ppm) through the Po(210) ionizer. In the ion−molecule region the SF_6^- reacted to near completion in the presence of excess O_3 to produce O_3^-:

$$SF_6^- + O_3 \rightarrow O_3^- + SF_6 \quad (6)$$

Thus, O_3^- became the primary reagent ion. The NO_2 was ionized through reaction with O_3^- to produce NO_3^-:

$$O_3^- + NO_2 \rightarrow NO_3^- + O_2 \quad (7)$$

The ions were detected with a quadrupole mass spectrometer in a two-stage differentially pumped vacuum chamber. Ion−molecule gases (neutrals and ions) were drawn into the front chamber by a mechanical pump (Varian SD-450). The ions were focused by a 4 cm o.d. and 0.1 mm i.d. stainless steel plate held at −50 V and passed into a second chamber which contained the quadrupole mass filter (ABB Extrel Merlin) pumped by a turbomolecular drag pump (Balzers TMU 520). The rear chamber, which held the multiplier assembly, was pumped by a second turbomolecular drag pump. Both turbomolecular drag pumps were backed by the same rotary pump (Varian SD-300). The rear chamber was typically at a pressure of $\sim 2 \times 10^{-6}$ Torr.

Measurement

Titration of Photofragments. To measure O(1D) yields, it is necessary to distinguish O(1D) from O(3P). This differentiation was made through the inclusion of a reactant which preferentially reacts with the O(1D). In this experiment an excess of N_2O ($[N_2O] \sim 100[O_3]$) was used because it reacts quickly with O(1D) but not with O(3P):

$$O(^1D) + N_2O \rightarrow NO + NO \quad (8)$$

$$\rightarrow N_2 + O_2 \quad (9)$$

The rate coefficients of reactions 8 and 9 are comparable, and reaction 9 represents a significant loss channel for the O(1D). However the production of two NO molecules in reaction 8 compensates for this loss. Once the NO has been formed it reacts with the O_3 which is present to form NO_2:

$$NO + O_3 \rightarrow NO_2 + O_2 \quad (10)$$

The NO_2 enters the ion−molecule region where O_3^- ionizes it to NO_3^- via reaction 7. Thus, the O(1D) photofragment was transformed into NO_3^- through a series of titration reactions.

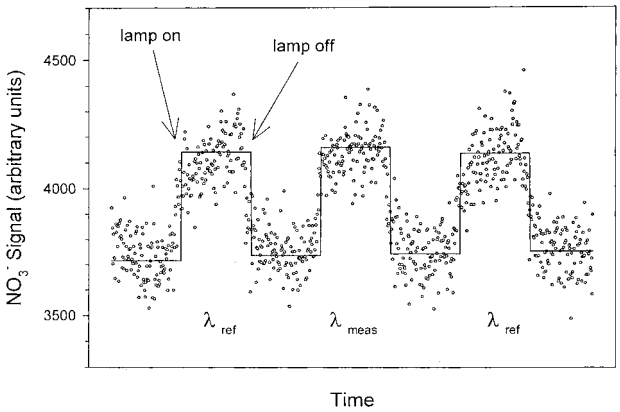

Figure 2. Sample signal rise for the detection of NO_3^- at reference (λ_{ref} = 300 nm) and measurement (λ_{meas}) wavelengths. The solid line represents an average of the signal with and without the photolysis light.

Relative quantum yield measurements were made by comparison of NO_3^- yields at various wavelengths relative to the yield at a reference wavelength, 300 nm. This reference wavelength was chosen for several crucial reasons. First, the O_3 absorption cross section is large at this wavelength (4×10^{-19} cm^2 at 298 K). Second, the O(1D) quantum yield is known to be close to unity (∼0.9) at this wavelength. Third, the O(1D) quantum yield is believed to be constant around this wavelength (thus minimizing errors incurred by slight wavelength shifts). All relative measurements were put on an absolute scale by normalizing the values measured at 308 nm to 0.79, as fixed by numerous previous studies.[4−6,12,13,15]

The wavelength of the light in the photolysis tube was alternated between the reference and measurement wavelengths (see Figure 2) by changing the angle of the diffraction grating in the monochromator. Measurements were typically made using an exposure time of 3 min at each wavelength. Since only the wavelength of the light was changed, this procedure allowed other variables (including gas flows and concentrations) to be kept constant between successive measurements. As the ozone was dissociated, concentrations of some of the trace species in the photolysis tube changed. If the effective rates of photolysis at the reference and measurement wavelengths were significantly different, then the secondary chemistry involving these trace species would be different, as well. To minimize the effects of this secondary chemistry on the species being measured, the NO_2 concentration (as measured by the NO_3^- signal) was

matched at the two wavelengths. Placement of a neutral density filter at the entrance slit of the monochromator allowed the light to be attenuated and the magnitude of the NO_3^- signal to be controlled. With comparable concentrations of all trace species at the two wavelengths, similar detection sensitivities and secondary chemistry were ensured. This procedure allowed a direct comparison of photolysis-titration product yields at the two wavelengths.

Calculation of Quantum Yields. The quantum yield at the measurement wavelength (λ_2) was calculated relative to that at the reference wavelength (λ_1) through the following expression:

$$\Phi_{\lambda_2} = \Phi_{\lambda_1} \frac{S_{\lambda_2}}{S_{\lambda_1}} \frac{I_{\lambda_1}}{I_{\lambda_2}} \frac{\lambda_1}{\lambda_2} \left[\frac{\exp(\sigma_{\lambda_1}[O_3]l) - 1}{\exp(\sigma_{\lambda_2}[O_3]l) - 1} \right] \qquad (11)$$

In this equation, S_λ is the NO_3^- signal rise, I_λ is the light flux (in Watts) measured by the calibrated photodiode and σ_λ is the O_3 absorption cross section reported previously by Molina and Molina.[16] The bracketed term at the end represents a correction for the attenuation of the light by O_3, where l is the length of the tube and the O_3 concentration is determined through UV absorption. The optical depth never exceeded a value of 0.3 with the O_3 concentrations and cross sections used in the experiments. In using the above expression it was assumed that both the O_3 concentration and the flow velocities of the gases remained constant between successive measurements. The error resulting from this assumption is negligible for all results presented here. A derivation of eq 11 is given in the Appendix.

The light exiting the monochromator encompasses a range of wavelengths about the central wavelength so that the light entering the photolysis tube is a function of wavelength, and I_λ becomes $I(\lambda)$. The wavelength distribution of the light is governed by the shape function of the monochromator which is determined by the geometries of the entrance and exit slits. In this case the shape function is triangular with maximum intensity at the central wavelength.

The shape and width of this distribution was verified in two separate experiments. In one test a second monochromator was coupled to the first monochromator and the intensity of the light was measured as a function of wavelength. In a second test the light flux from a narrow emission line of a mercury pen lamp was measured as the monochromator was scanned about the emission wavelength. Both of these tests confirmed the triangular shape and the expected width of the monochromator shape function. Because the absorption cross section is also a function of wavelength eq 11 cannot be used directly. Instead, both the numerator and the denominator in the equation must be integrated numerically over the appropriate wavelength ranges, and precise knowledge of the shape function as well as high-resolution cross section data[16] are required to accomplish this.

Equation 11 was used to calculate $O(^1D)$ quantum yields for measurements made from 295 to 338 nm. Measurements were made at temperatures of 226, 263, and 298 K (±3 K) at a pressure of 50 Torr. Table 1 lists the quantum yields measured at 298 K and Table 2 lists the quantum yields measured at 226 and 263 K (all normalized to a value of 0.79 at 308 nm). The slit width of the monochromator (and thus the wavelength bandwidth) was increased at longer wavelengths to compensate in part for the accompanying decrease in the O_3 absorption cross section. The wavelength bandwidth varied from ±0.05 nm to ±1.80 nm, where the bandwidth is defined as the full width at half-maximum (fwhm). It should be noted that the full range of wavelengths exiting the monochromator was twice as large (encompassing ±2 fwhm). The quantum yields reported represent a weighted average (as per the monochromator shape function and the absorption cross section) over the corresponding wavelength range.

TABLE 1: Room Temperature $O(^1D)$ Quantum Yields Measured in This Work[a]

λ (nm)	$\Delta\lambda$[b] (nm)	Φ (298 K)
295	±0.22	0.88 ± 0.03
297.5	±0.22	0.91 ± 0.05
300	±0.11	0.86 ± 0.03
301	±0.22	0.87 ± 0.08
302	±0.22	0.90 ± 0.06
303	± 0.22	0.89 ± 0.05
304	± 0.22	0.94 ± 0.10
305	± 0.11	0.94 ± 0.03
306	± 0.05	0.84 ± 0.10
307	± 0.05	0.80 ± 0.12
308[c]		0.79
309	±0.05	0.70 ± 0.07
310	±0.11	0.62 ± 0.09
311	±0.11	0.44 ± 0.06
312	±0.11	0.35 ± 0.02
313	±0.11	0.34 ± 0.05
314	±0.11	0.27 ± 0.05
315	±0.22	0.22 ± 0.03
316	±0.56	0.28 ± 0.01
317	±0.56	0.26 ± 0.05
318	±0.56	0.24 ± 0.02
319	±1.12	0.27 ± 0.03
320	±0.56	0.19 ± 0.01
321	±0.56	0.17 ± 0.04
322	±0.56	0.15 ± 0.01
323	±0.56	0.13 ± 0.03
324	±0.56	0.13 ± 0.04
325	±1.12	0.11 ± 0.01
326	±1.12	0.10 ± 0.01
327	±1.12	0.10 ± 0.02
328	±1.12	0.12 ± 0.03
329	±1.12	0.08 ± 0.02
330	±1.12	0.12 ± 0.03
331	±1.12	0.15 ± 0.03
334	±1.80	0.13 ± 0.03
335	±1.12	0.13 ± 0.02
337	±1.80	0.11 ± 0.03
338	±1.12	0.11 ± 0.04

[a] Quoted errors represent 95% confidence intervals. [b] $\Delta\lambda$ = fwhm. [c] Normalization wavelength.

TABLE 2: Cold Temperature $O(^1D)$ Quantum Yields Measured in This Work[a]

λ (nm)	$\Delta\lambda$[b] (nm)	Φ (263 K)	Φ (226 K)
312	±0.22	0.24 ± 0.03	0.17 ± 0.03
316	±0.56	0.15 ± 0.04	0.11 ± 0.03
320	±0.56	0.11 ± 0.02	0.08 ± 0.01
324	±1.12	0.11 ± 0.02	0.09 ± 0.02
328	±1.12	0.11 ± 0.03	0.10 ± 0.01
331	±1.12	0.13 ± 0.01	0.14 ± 0.02
334	±1.80	0.11 ± 0.01	0.12 ± 0.02
337	±1.80	0.13 ± 0.02	0.13 ± 0.02

[a] Quoted errors represent 95% confidence intervals. [b] $\Delta\lambda$ = fwhm.

The dramatic decrease in the cross section (e.g., σ_{338} is more than 5000 times smaller than σ_{254}) means that a small amount of stray light of short wavelength could contribute a significant fraction of the $O(^1D)$ produced. To minimize such effects, a long-pass filter (centered about 300 nm) was used in all measurements at wavelengths longer than 300 nm. In addition, we measured the stray light as a function of wavelength through the coupling of a second monochromator (ARC VM-503, 3600 lines/mm) to the first one. From these measurements we were

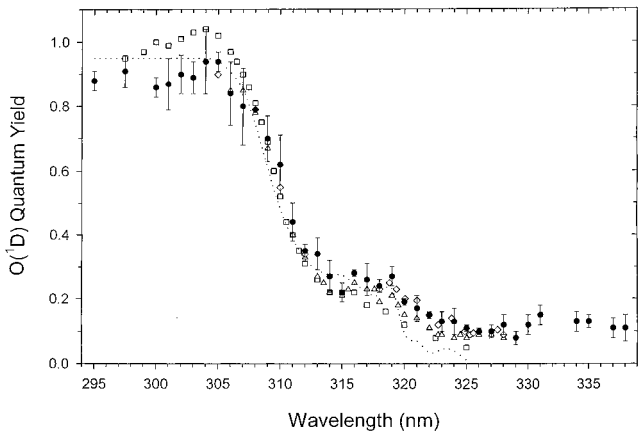

Figure 3. O(1D) quantum yields as a function of wavelength from 295 to 338 nm at 298 K: (●) this work; (□) Brock and Watson[4] (1980); (△) Talukdar et al.[12] (1998); (◇) Takahashi et al.[13] (1998); (•••) DeMore et al.[17] (1997). Error bars shown represent 95% confidence limits.

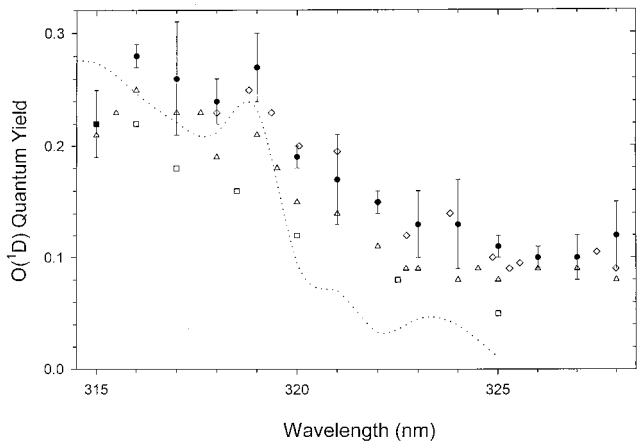

Figure 4. O(1D) quantum yields as a function of wavelength in the tail region at 298 K: (●) this work; (□) Brock and Watson[4] (1980); (△) Talukdar et al.[12] (1998); (◇) Takahashi et al.[13] (1998); (•••) DeMore et al.[17] (1997). Error bars shown represent 95% confidence limits.

able to determine that the amount of short wavelength stray light was negligible even considering the increased cross sections at those wavelengths. Therefore, we are confident that the observed NO_3^- signal rises could not have resulted from photolysis by short wavelength stray light and must be attributable to the production of O(1D) by photolysis at the selected measurement wavelengths. As evident in Figure 2, there is a "dark" NO_3^- background signal in the measurements; it may originate from a small HNO_3 contamination present in the curing process used in the production of the Po^{210} ionization source. This background HNO_3 should not interfere with the ionization chemistry, as the reaction time in the ionization region is short (∼5 ms). In addition, the signal is modulated with the photolysis light and relative changes in the signal are measurable as long as the dark signal remains constant.

Figure 3 shows the data obtained at 298 K over the entire range of wavelengths studied along with data from other studies[4,12,13,17] for comparison. The uncertainties shown represent 95% confidence limits and include estimated uncertainties in the measurement of the light flux as well as estimated uncertainties in the O_3 absorption cross sections.[16] The behavior of the quantum yield data in the "tail" region (315 nm ≤ λ ≤ 328 nm) can be seen in Figure 4, and the temperature dependence of the quantum yield is evident in the 226−298 K data shown in Figure 5.

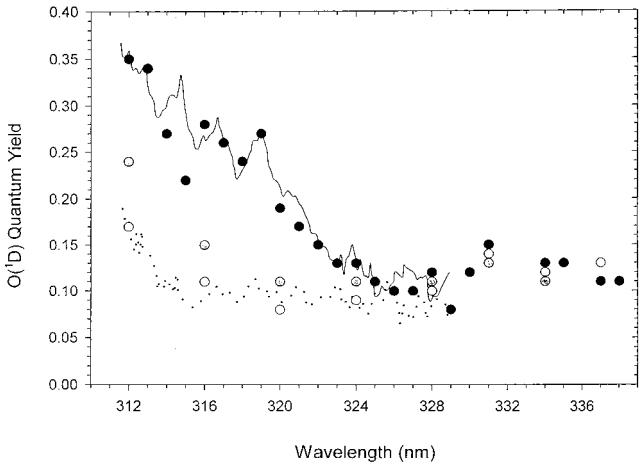

Figure 5. O(1D) quantum yields at various temperatures: (○) 226 K; (gray circles) 263 K; (●) 298 K. Lines representing (smoothed) data from Takahashi et al.[13] are shown for comparison: (•••) 223 K, (—) 298 K.

Discussion

Results. The O(1D) quantum yields measured in this study support values greater than zero at wavelengths up to 338 nm at temperatures from 226 to 298 K. These measurements agree qualitatively with recent work[9,10,12,13] and have contributed to the identification of a nonzero quantum yield well into the tail region of the spectrum. However, the values we obtained in this region are significantly larger than those reported from the other recent studies. In addition, the origin of O(1D) production at these wavelengths has remained a topic of interest, and our quantum yield measurements made over a range of temperatures have aided in the interpretation of O(1D) production from O_3 photolysis.

The quantum yields at long wavelengths have been attributed to contributions from vibrational excitation of O_3 and the formation of spin-forbidden products (reaction 2). The recommendation of DeMore et al.[17] (JPL-97) is based on a model by Michelsen et al.[19] in which vibrational excitation of the symmetric, asymmetric and bending modes of O_3 is included. The effect of this "hot O_3" contribution on the quantum yield (shown in Figure 4) can be seen with distinct structure appearing near 319, 321, and 323 nm. This structure can also be seen in the data from this study and that of Takahashi et al.,[13] as well as that of Talukdar et al.[12] to a lesser degree. In addition, the effect of temperature on the population of the excited modes can be seen in the decrease of the quantum yield at colder temperatures (Figure 5). Therefore, it seems reasonable to conclude that internal excitation of vibrational modes in the O_3 accounts for a fraction of the long-wavelength O(1D) production.

However, at wavelengths greater than 325 nm (where more than one quantum of vibrational energy would be needed) and at temperatures below 298 K the importance of hot O_3 contribution to production of O(1D) should diminish. Observations of nonzero values at wavelengths greater than 325 nm and at temperatures below room temperature suggest that hot O_3 is not the only source of O(1D) and that a spin-forbidden process must be active. The data of Takahashi et al.[13] at 298 and 223 K indicate a convergence near 328 nm (shown in Figure 5), implying production of O(1D) that is independent of temperature at longer wavelengths. Our results corroborate this convergence indicating a nearly constant O(1D) quantum yield (∼0.12) at wavelengths from 325 to 338 nm and over a temperature range 226−298 K. These findings are consistent

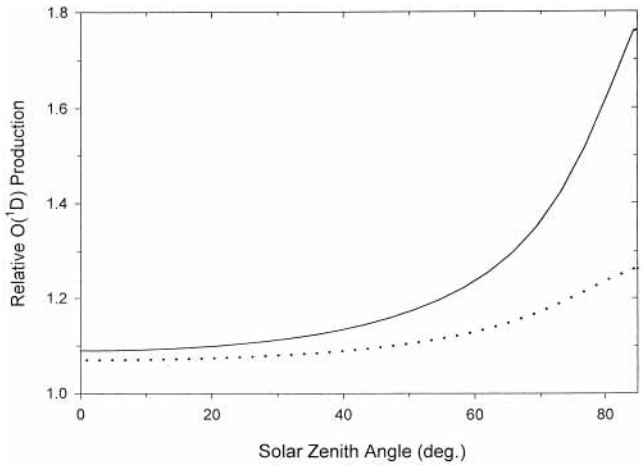

Figure 6. O(^{1}D) production rates calculated for the earth's surface with 330 DU of overhead ozone[21] relative to rates estimated with quantum yield recommendations of DeMore et al.[17] (JPL-97) (—) and Sander et al.[18] (JPL-2000) (···).

with a spin-forbidden production of O(^{1}D) at longer wavelengths, although the value of 0.12 is higher than that suggested by Takahashi et al. (0.08)[13] and Talukdar et al. (0.06).[12]

The quantum yields at 300 nm $\leq \lambda \leq$ 310 nm reported in this study also indicate some structure with a peak around 304—305 nm. This same structure has been observed in previous studies[4,6,7] although it was not included in the recommendation of DeMore et al.[17] In fact, an average value of 0.95 is recommended for 290 nm $\leq \lambda \leq$ 305 nm which seems to be a slight overestimation when compared to the data obtained in this study. Although the differences in the shape and values of the quantum yield at these wavelengths might not significantly alter calculations of the overall production of O(^{1}D) in the atmosphere, they could affect laboratory studies which normalize relative measurements of O(^{1}D) to values at these short wavelengths.

After the work presented in this paper was completed, we learned that Bauer et al.[20] have recently completed additional measurements of the O(^{1}D) quantum yield. They used laser-induced fluorescence of vibrationally excited OH—produced from reaction of O(^{1}D) with H_2 or CH_4—to measure the quantum yield from 305 to 375 nm at 295 K and from 305 to 340 nm at 273 K. They found a nearly constant quantum yield independent of temperature at wavelengths longer than about 325 nm. Though these findings are qualitatively in good agreement with our measurements, the values in the tail region are approximately a factor of 2 lower than our measurements.

Atmospheric Implications. Although the absorption cross section of O_3 decreases rapidly at wavelengths in the tail region ($\lambda >$ 315 nm), the intensity of the actinic flux increases rapidly over the same region of the spectrum. A small but measurable O(^{1}D) quantum yield at these wavelengths could therefore imply a significant yield of O(^{1}D) and lead to an enhancement in calculated production in the lower atmosphere in comparison with previous estimates. The effect of including the O(^{1}D) quantum yield data from this work is shown in Figure 6 as an increase in calculated O(^{1}D) production at the earth's surface relative to identical calculations using the recommendations of DeMore et al.[17] (JPL-97) and Sander et al.[18] (JPL-2000). The sharp increase observed for solar zenith angles above 60 degrees can be attributed to the effective filtering of shorter wavelength radiation by overhead O_3 at these angles. In this way the actinic flux reaching the earth is selectively enhanced at longer wavelengths, precisely where our data deviate most from previous studies. Similar increases in O(^{1}D) production are expected at higher altitudes, however the sparseness in the cold temperature data of this study precludes such detailed calculations. Although measurements at wavelengths longer than 338 nm might offer insight into the processes controlling the photodissociation of O_3, our calculations show that radiation at wavelengths above 338 nm contributes very little to O(^{1}D) production in the lower atmosphere.

Conclusion

The results of our experiments with O_3 photolysis in conjunction with other studies[12,13,20] suggest that two processes contribute to the production of O(^{1}D) at wavelengths beyond its thermodynamic threshold. First, structure and temperature dependence in the quantum yield at long wavelengths offer evidence that internally excited O_3 can extend dissociation via reaction 1 beyond the 310 nm threshold. Second, a nearly constant quantum yield (~0.12) independent of temperature from 325 to 338 nm supports the participation of the spin-forbidden channel, reaction 2, at these wavelengths. We estimate that utilization of our quantum yield data leads to a significant enhancement in the calculated O(^{1}D)—and thus OH—production in the lower atmosphere, especially at high solar zenith angles where production rates are as much as 75% higher than those based on the quantum yield recommendation of DeMore et al.[17]

Appendix

Equation 11 is derived from the comparison of photofragment yields based on the calculated dissociation rates:

$$\frac{\mathrm{d}[\mathrm{O}(^1\mathrm{D})]}{\mathrm{d}t} = j(\lambda,t)[\mathrm{O_3}]\,\Phi(\lambda)$$

The absorption rate coefficient, $j(\lambda,t)$, is calculated from the light flux, I (in Watts), measured at the exit of the photolysis tube, the cross section of the tube, A (in cm^2), and the energy per photon, $h\nu$ (in Joules):

$$j(\lambda,t) = \frac{I\sigma}{Ah\nu}$$

The amount of O(^{1}D) produced from photolysis can then be calculated by integrating over the residence time, t, in the photolysis tube:

$$\begin{aligned}\Delta[\mathrm{O}(^1\mathrm{D})] &= \Phi[\mathrm{O_3}]\int_0^t \frac{I\sigma\lambda}{Ahc}\,\mathrm{d}t \qquad \left(\nu = \frac{c}{\lambda}\right)\\ &= \Phi\frac{[\mathrm{O_3}]}{v}\int_0^l \frac{I\sigma\lambda}{Ahc}\,\mathrm{d}x \qquad \left(t = \frac{x}{v}\right)\\ &= \Phi\frac{[\mathrm{O_3}]}{v}\int_0^l \frac{I_0\sigma\lambda}{Ahc}e^{-\sigma[\mathrm{O_3}]x}\,\mathrm{d}x\end{aligned}$$

where v is the flow velocity, l is the length of the tube and Beer's law is used to express I as a function of distance along the tube (I_0 is the light flux entering the tube). The use of Beer's law is valid under all conditions employed with a maximum optical depth of 0.3. The integral can now be evaluated and the resulting expression simplified again with the use of Beer's law:

$$\begin{aligned}\Delta[\mathrm{O}(^1\mathrm{D})] &= \Phi\frac{I_0\lambda}{Ahcv}[1 - \mathrm{e}^{-\sigma[\mathrm{O_3}]l}]\\ &= \Phi\frac{I\lambda}{Ahcv}[\mathrm{e}^{\sigma[\mathrm{O_3}]l} - 1]\end{aligned}$$

The NO_3^- signal rise from the mass spectrometer, S_λ, is proportional to $\Delta[O(^1D)]$ at both the reference (λ_1) and measurement (λ_2) wavelengths:

$$S_{\lambda_1} = a\Phi_{\lambda_1}\frac{I_{\lambda_1}\lambda_1}{\upsilon_1}[\exp(\sigma_{\lambda_1}[O_3]_1 l) - 1]$$

$$S_{\lambda_2} = a\Phi_{\lambda_2}\frac{I_{\lambda_2}\lambda_2}{\upsilon_2}[\exp(\sigma_{\lambda_2}[O_3]_2 l) - 1]$$

Since a is the proportionality constant:

$$\frac{1}{\Phi_{\lambda_1}}\frac{S_{\lambda_1}\upsilon_1}{I_{\lambda_1}\lambda_1}\frac{1}{[\exp(\sigma_{\lambda_1}[O_3]_1 l) - 1]} = \frac{1}{\Phi_{\lambda_2}}\frac{S_{\lambda_2}\upsilon_2}{I_{\lambda_2}\lambda_2}\frac{1}{[\exp(\sigma_{\lambda_2}[O_3]_2 l) - 1]}$$

$$\Phi_{\lambda_2} = \Phi_{\lambda_1}\frac{S_{\lambda_2}}{S_{\lambda_1}}\frac{\upsilon_2}{\upsilon_1}\frac{I_{\lambda_1}}{I_{\lambda_2}}\frac{\lambda_1}{\lambda_2}\frac{[\exp(\sigma_{\lambda_1}[O_3]_1 l) - 1]}{[\exp(\sigma_{\lambda_2}[O_3]_2 l) - 1]}$$

Assuming $\upsilon_2 = \upsilon_1$ and $[O_3]_2 = [O_3]_1$ (i.e., flow velocities and O_3 concentrations are constant between successive measurements at the two wavelengths):

$$\Rightarrow \Phi_{\lambda_2} = \Phi_{\lambda_1}\frac{S_{\lambda_2}}{S_{\lambda_1}}\frac{I_{\lambda_1}}{I_{\lambda_2}}\frac{\lambda_1}{\lambda_2}\frac{[\exp(\sigma_{\lambda_1}[O_3] l) - 1]}{[\exp(\sigma_{\lambda_2}[O_3] l) - 1]} \qquad (11)$$

Acknowledgment. This research is supported by a grant from the National Aeronautics and Space Administration Upper Atmosphere Research Program. We thank Mathew Evans for help with the modeling of tropospheric O(^{1}D) production and Carl Percival for assistance with initial work involving the slow-flow system. G.D.S. acknowledges partial support from the NSF Training Grant in Environmental Chemistry.

References and Notes

(1) Ravishankara, A. R.; Hancock, G.; Kawasaki, M.; Matsumi, Y. *Science* **1998**, *280*, 60.

(2) Arnold, I.; Comes, F. J.; Moortgat, G. K. *Chem. Phys.* **1977**, *24*, 211.

(3) Philen, D. L.; Watson, R. T.; Davis, D. D. *J. Phys. Chem.* **1977**, *67*, 3316.

(4) Brock, J. C.; Watson, R. T. *Chem. Phys.* **1980**, *46*, 477.

(5) Greenblatt, G. D.; Wiesenfeld, J. R. *J. Chem. Phys.* **1983**, *78*, 4924.

(6) Trolier, M.; Wiesenfeld, J. R. *J. Geophys. Res.* **1988**, *93*, 7119.

(7) Armerding, W.; Comes, F. J.; Schülke, B. *J. Phys. Chem.* **1995**, *99*, 3137.

(8) Richter, R. C.; Hynes, A. J. *J. Phys. Chem.* **1996**, *100*, 8061.

(9) Silvente, E.; Ricther, R. C.; Zheng, M.; Saltzman, E. S.; Hynes, A. J. *Chem. Phys. Lett.* **1997**, *264*, 309.

(10) Ball, S. M.; Hancock, G.; Martin, S. E.; Pinot de Moira, J. C. *Chem. Phys. Lett.* **1997**, *264*, 531.

(11) Denzer, W.; Hancock, G.; Pinot de Moira, J. C.; Tyley, P. L. *Chem. Phys.* **1998**, *231*, 109.

(12) Talukdar, R. K.; Longfellow, C. A.; Gilles, M. K.; Ravishankara, A. R. *Geophys. Res. Lett.* **1998**, *25*, 143.

(13) Takahashi, K.; Taniguchi, N.; Matsumi, Y.; Kawasaki, M.; Ashfold, M. N. R. *J. Chem. Phys.* **1998**, *108*, 7161.

(14) Percival, C. J.; Smith, G. D.; Molina, L. T.; Molina, M. J. *J. Phys. Chem. A* **1997**, *101*, 8830.

(15) Talukdar, R. K.; Gilles, M. A.; Battin-Leclerc, F.; Ravishankara, A. R. *Geophys. Res. Lett.* **1997**, *24*, 1091.

(16) Molina, L. T.; Molina, M. J. *J. Geophys. Res.* **1986**, *91*, 14,501. Note: High-resolution cross section values were taken from the (unpublished) raw data from this work.

(17) DeMore, W. B.; Sander, S. P.; Golden, D. M.; Hampson, R. F.; Kurylo, M. J.; Howard, C. J.; Ravishankara, A. R.; Kolb, C. E.; Molina, M. J. NASA Panel for Data Evaluation. *Chemical Kinetics and Photochemical Data for Use in Stratospheric Modeling*; JPL Publication 97-4; JPL: Pasadena, CA, 1997.

(18) Sander, S. P.; Friedl, R. R.; Huie, R. E.; Kurylo, M. J.; Kolb, C. E.; Golden, D. M.; Ravishankara, A. R.; Molina, M. J. NASA Panel for Data Evaluation. *Chemical Kinetics and Photochemical Data for Stratospheric Modeling*; JPL Publication 00-3; JPL: Pasadena, CA, 2000.

(19) Michelsen, H. A.; Salawtich, R. J.; Wennberg, P. O.; Anderson, J. G. *Geophys.. Res. Lett.* **1994**, *21*, 2227.

(20) Bauer, D.; D'Ottone, L.; Hynes, A. J. *Phys. Chem. Chem. Phys.* **2000**, *2*, 1421.

(21) Using the NCAT TUV radiative transfer code version 4.0.